ADVANCED FUNCTIONAL MATERIALS
www.afm-journal.de

Sustainable Catalyst-Free PLG Networks: Recyclability, Biodegradability, and Functional Performance

*Lars Schwarzer, Emilia Fulajtar, and Seema Agarwal**

Recycling of thermosets remains a challenge, as their permanent networks prevent reprocessing and lead to persistent waste and microplastic pollution. As a potential solution, covalent adaptable networks (CANs) offer reprocessability through dynamic bond-exchange reactions but typically rely on toxic additives (organometallic catalysts) raising concerns about leaching and environmental persistence. To advance beyond recyclability alone, CANs can be designed with biodegradable polymer backbones, creating materials that not only allow reprocessing but also undergo degradation, thereby reducing environmental risks and microplastic pollution from accidental release. Here, a catalyst-free, biodegradable CAN based on star-shaped poly(lactide-*co*-glycolide) (PLG) cross-linked with pyromellitic dianhydride is reported, which introduces internal carboxylic acid groups to drive transesterification. The resulting networks exhibit high gel content (≈95%), mechanical performance comparable to poly(*L*-lactide) (Young's modulus ≈1.6 GPa), and complete retention of stiffness after thermal recycling. Stress-relaxation analysis confirms Arrhenius-like dynamics with an activation energy of 119 kJ mol^{-1}, consistent with reversible anhydride exchange. The PLG CAN also demonstrates rapid biodegradation (>60% within 25 days in compost) and functional properties including robust shape-memory and applicability as reusable adhesive (60 mg film supporting 6.3 kg load). This work establishes biodegradable, catalyst-free CANs as a sustainable materials platform, uniting mechanical robustness, reprocessability, and environmentally benign degradation.

1. Introduction

Modern polymer applications increasingly demand mechanically robust and durable materials, particularly thermosets. These materials owe their superior properties to permanent covalent cross-linking; however, this same feature renders them nearly impossible to recycle, leading to substantial environmental concerns. In 2023, global plastic production reached 413.8 Mt, with thermosets accounting for ≈14% of the total.[1] Conventional thermoplastic recycling methods cannot be applied to thermosets, while alternative approaches such as chemical, mechanical, or pyrolytic recycling are typically cost- and energy-intensive.[2–4] As a result, thermoset waste is predominantly managed through regulated incineration, landfilling, or unregulated environmental release, all of which contribute to significant environmental pollution and creation of microplastics.

This class of polymer material would benefit from the concept of covalent adaptable networks (CANs), which provide thermosets with dynamic, reversible covalent bonds that enable reprocessability and recyclability like thermoplastics.[5,6] These dynamic networks rely on bond exchange reactions at higher temperatures spanning a wide range of different possible reactions, like transesterification,[7–10] transcarbamoylation or urethane exchange,[11–14] imine bond exchange,[15,16] transamination of vinylogous urethanes,[17–19] disulfide exchange,[20,21] or siloxane exchange.[22,23] These systems usually require some sort of external catalyst that enables exchange reactions. Catalysts for this purpose range from metal organic compounds to strong organic bases or acids,[24–26] common examples are zinc- or tin-based Lewis acids for transesterification reactions.[10,11] The major disadvantages of external catalysts include their toxicity, corrosiveness, and environmental hazards, raising concerns about safety, leaching, and long-term stability. A critical conceptual advance in this regard is the concept of an internal catalyst, in which catalytic groups are covalently embedded into the polymer network.[17,27,28] The catalytically active group may be immobilized on the polymer backbone in its already active form, thus preventing issues like leaching or agglomeration. Alternatively, weaker groups like amines[29] or carboxylic acids[30] can act as a catalyst based on proximity to reversible bonds through a variety of possible synergistic effects. This behavior is generally known in organic chemistry as the neighboring group effect (NGE), where the reaction rate of a specific reaction is greatly increased by the participation of a neighboring group.

L. Schwarzer, E. Fulajtar, S. Agarwal
Advanced Sustainable Polymers, MC2
University of Bayreuth
95440 Bayreuth, Germany
E-mail: agarwal@uni-bayreuth.de

S. Agarwal
Bavarian Polymer Institute
University of Bayreuth
95440 Bayreuth, Germany

The ORCID identification number(s) for the author(s) of this article can be found under https://doi.org/10.1002/adfm.202527257

DOI: 10.1002/adfm.202527257

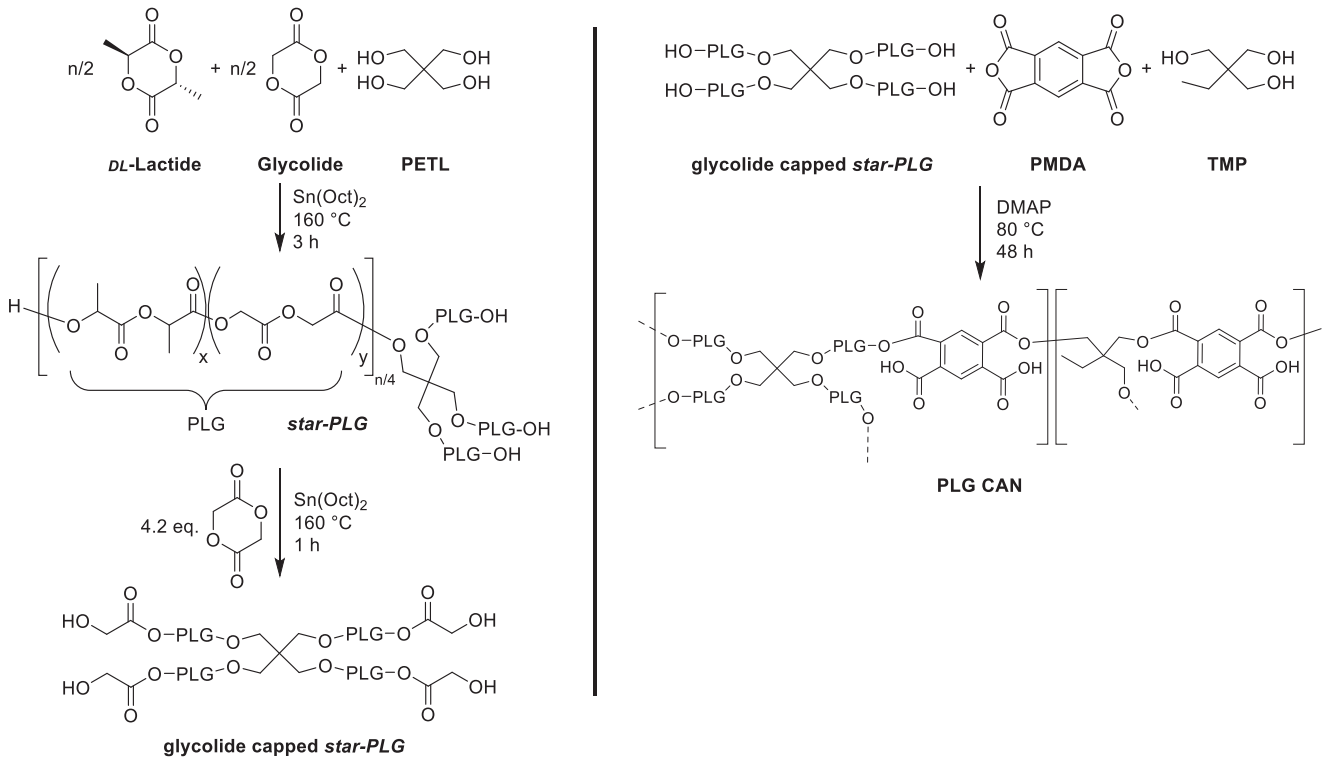

Scheme 1. Complete synthetic route to poly(lactide-*co*-glycolide) covalent adaptable network starting from star-shaped PLG.

The group of Delahaye et al. introduced a CAN design where dynamic transesterification is internally enabled by sterically fixed neighboring carboxylic acid groups, resulting in a robust, recyclable network without additional catalyst.[30] Their starting material, pyromellitic dianhydride (PMDA), reacts readily with small molecules with free-hydroxy groups to form bifunctional phthalic monoesters, or phthalic bis(monoester), that carry a free carboxylic acid group in the ortho position to an ester group. They proved the dissociative mechanism of bond exchange through reformation of the anhydride ring at high temperature, which upon cooling reacts with available alcohols to reform the monoester functionality with free carboxyl groups.[30] During dissociative network rearrangements, the network initially collapses and enters a flowing state, before reestablishing bonds and reforming the network. CANs that follow an associative mechanism are also called vitrimers. In this case, free functional groups (e.g., alcohol or amine) add to the existing bond and form a transition state before cleaving the old bond and releasing a new free functional group.[17,18,31]

We hypothesized that applying the established phthalic bis(monoester) transesterification system obtained from anhydride opening of PMDA with hydroxy terminated star-shaped poly(lactide-*co*-glycolide) (PLG) would enable the design of a biodegradable CAN. PLG is an amorphous polymer known for its biocompatibility and degradation in diverse environments,[32–34] but its low glass transition temperature ($T_g \approx 45$–55 °C)[35] severely limits practical applications. By introducing dynamic covalent cross-links, we expected to enhance the unfavorable thermomechanical properties that otherwise restrict linear PLG, while simultaneously retaining its recyclability and inherent degradability. In contrast, permanent cross-linking of PLG would sacrifice its recyclability, as is the case for conventional thermosets. Embedding degradability into the CAN backbone would further ensure non-persistence as microplastic, even in cases of intentional or accidental release. Therefore, star-shaped PLG with four arms was synthesized and fully characterized. The cross-linked network was formed by gelation of PLG with PMDA, establishing bifunctional phthalate monoesters and free carboxylic groups. Comprehensive characterization was performed on the PLG covalent adaptable network (PLG CAN). The materials dynamic properties were assessed by stress-relaxation experiments and related to the Arrhenius equation. Biodegradation was evaluated under composting conditions, and the film's potential as a recoverable adhesive and shape-memory polymer was investigated.

2. Results and Discussion

Star-shaped PLG was synthesized as the core cross-linking molecule. It carries terminal OH-groups that should react with added PMDA to form the desired cross-linked network with free carboxylic acid groups (**Scheme 1**). These carboxyl groups take part in dynamic bond-exchanges via transesterification reactions during (re-)processing. The synthesis followed a standard metal-catalyzed ring-opening polymerization mechanism using tin(II) octoate as catalyst and pentaerythritol (PETL) as initiator in the presence of lactide and glycolide.[36] After network formation, the catalyst was removed by double precipitation, first in methanol and then in *n*-pentane. The residual catalyst content in the network after purification was determined by measuring tin via

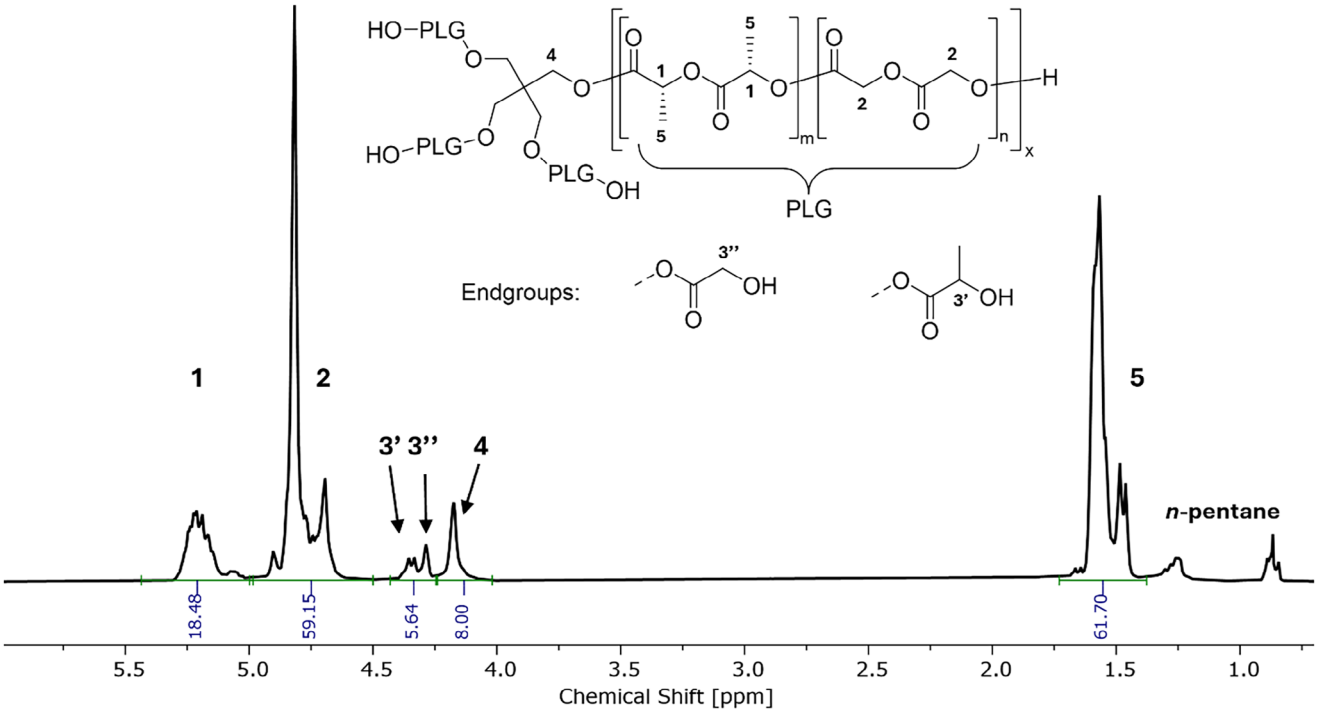

Figure 1. ^{1}H-NMR spectrum of star-shaped PLG in $CDCl_3$ recorded at 300 MHz.

inductively coupled plasma optical emission spectroscopy and found to be 0.006 wt.%, well below the typical catalyst loadings in vitrimer systems (0.05–2 wt.%). Therefore, it is not expected to exhibit any significant activity in the presented network.

The successful synthesis of star-shaped PLG macromonomer was confirmed by ^{1}H-NMR and FTIR. Further analysis of the macromonomer was carried out by GPC, TGA, and DSC. Additionally, the number of OH-groups was chemically quantified by converting the free hydroxy groups of the macromonomer into benzoyl esters through the reaction with benzoyl chloride. The average number of OH-groups was then confirmed by ^{1}H-NMR to 3.8 by dividing the integral of the newly formed aromatic esters, referenced to the core PETL proton signal, by the number of protons of each ring which is five (Figure S4, p. S4, Supporting Information). In the ^{1}H-NMR spectrum, the main visible features include the methine (—CH—) protons at 5.25 ppm of the opened lactide units, the methylene (—CH_2—) protons at 4.75 ppm of the glycolide rings, the lactide methyl (—CH_3) groups at 1.5 ppm, appearing in a 3:1 ratio to the methine signal. The core PETL (—CH_2—) groups are observed at 4.17 ppm, close to the visible hydroxyl carrying end group signals between 4.2 and 4.4 ppm (**Figure 1**). These later signals can be assigned to the two different end-groups formed during ring-opening: the methine group of lactide (4.35 ppm) and the methylene group of glycolide (4.28 ppm), attached to the terminal OH-group. The NMR also reveals that every macromonomer shows four OH carrying end-groups on average, one for each arm.

By deconvolution of the overlapping signals and referencing the PETL core, the average number of hydroxyl chain ends originating from lactide or glycolide ring-opening was determined to be in a 1:1 molar ratio. Without the additional glycolide introduced after the initial polymerization, this ratio was 3:1, with secondary hydroxyl chain ends predominantly derived from lactide (Figure S8, Supporting Information). The higher fraction of primary hydroxyl groups generated from glycolide ring-opening facilitated improved gel formation in the subsequent cross-linking step (up to 95% after processing) as described in the next section. In contrast, networks formed with mostly secondary hydroxyl chain ends from lactide yielded gel contents of only ≈60% post processing after multiple attempts. This might be attributed to the higher reactivity of the primary chain-end hydroxyl groups derived from glycolide compared to the secondary hydroxyl groups originating from lactide during the anhydride-based network formation step.

This likely results from the lower reactivity of secondary alcohols compared to primary alcohols and steric hindrance due to the methyl group in the lactide chain-ends. Especially since the formed carboxylic acid ortho ester in the network is also very bulky and stiff. GPC was used to determine the polymer dispersity (≈1.2) but is unreliable for molar mass due to the star-shape of the macromonomer (Figure S1, Supporting Information). The molecular weight of the macromonomer was determined through ^{1}H-NMR data by calculating the average number of repeating units for the PLG. Initially, the PETL core is referenced with all four CH_2 groups. By integration of the lactide methine (5.25 ppm) and glycolide methylene (4.75 ppm) regions, the number of lactide and glycolide units can be calculated. The molecular weight is then calculated by using the monomer molecular weights. The PLG in Figure 1 has therefore an average molecular weight of ≈3300 g mol^{-1} (see p. S3, Supporting Information).

The next step was the network formation by the reaction of hydroxy-chain end functionalized star-shaped PLG macromonomer and TMP with PMDA. Under the given reaction conditions, it is expected that the OH-groups of PLG macromonomer and TMP react with PMDA anhydrides leading to new ester linkages and the free carboxylic acid groups. The networks were extracted with THF for 24 h to remove any unreacted components. The network showed the disappearance of the OH-absorption band in the IR spectrum at ≈3500 cm^{-1} (**Figure 2A**). New groups that are introduced into the polymer are the formed carboxylic acids, which result in a very broad absorption band over a wide range of ≈2250–3750 cm^{-1}. Another new band appears at ≈800 cm^{-1} that can be attributed to the aromatic C—H vibrations of the tetra substituted aromatic unit of the PMDA. The overall intensity of the PMDA absorption bands (both C—H and COOH vibrations) appears low due to the very intense carbonyl band at ≈1750 cm^{-1} of the C═O vibrations of both the incorporated PLG macromonomer and the newly formed aromatic esters, the relatively low concentration of PMDA in the polymer network (20 wt.%), and overall low absorption of the material. Thus, further proof of the successful incorporation of PMDA into the network is obtained by solid-state ^{13}C-NMR (Figure 2C). The PLG backbone is visible through the carbonyl carbon signal (1) at 167 ppm, the shifted shoulder is attributed to the slight differences of lactide and glycolide carbonyl carbon.[11] Glycolide methylene (4) and lactide methine (3) carbons give signals at 61 and 69 ppm, respectively, the lactide methyl group (7) is observed at 16 ppm. Additional visible carbons include the methylene (6) and methyl (8) group of the used TMP at 26 and 7 ppm, the PETL methylene groups (5) at 42 ppm, and the incorporated aromatic hydrogen bearing carbons (2) at 131 ppm. No carboxylate carbons and substituted aromatic carbons are visible due to experimental limitations of the cross-polarization technique in hydrogen deficient regions. Nonetheless, this confirms the structure of the PLG network and the successful incorporation of PMDA as linker.

The network formation is also reflected in the thermal properties of the neat PLG macromonomer compared to the PLG CAN (Figure 2B). Linear PLG usually exhibits a glass transition temperature T_g of ≈45–50 °C, whereas, the star-shaped PLGs' are reduced to 30–35 °C.[11,37] By cross-linking to form the network it is expected that the chain mobility of the macromonomer PLG is greatly reduced and therefore the T_g increases. The DSC experiments show a clear shift to higher temperatures in all curves after network formation at almost twice the initial value. The degradation behavior also changed indicated by the onset degradation temperature increasing by ≈50 °C from PLG macromonomer to PLG CAN (Figures S2 and S5, Supporting Information).

For the material to be considered a covalent adaptable network it must follow an Arrhenius like relaxation behavior. This means that the material dissipates applied stress not through molecular motion, as is the case for non-cross-linked thermoplastics, but through chemical exchange reactions.[6,38] This was observable through stress-relaxation experiments using rheology under constant strain, as depicted in **Figure 3A**.

Most thermoplastic materials will relax through molecular motion immediately after being set under stress. This will be visible in the relaxation curve by a constant decline in the relaxation modulus until the material is eventually fully relaxed, following the known William–Landel–Ferry equation.[39] Irreversible cross-linked thermosets do not relax. In contrast, reversible cross-linked polymers behave differently, showing an initial plateau that shifts to an exponential decay after a certain time. First, the network is fully cross-linked and exhibits no relaxation. After a certain period, however, dynamic bond-exchange reactions begin, leading to bond cleavage and reformation, which enable network rearrangement and stress relaxation. Since this relaxation does not rely on macromolecular motion as the main relaxation tool, but chemical exchange reactions, it can be correlated to the Arrhenius law (see p. S7, Supporting Information). The resulting Arrhenius relation is depicted in Figure 3B. This shows that the cross-linked material is capable of full Arrhenius-like relaxation based on a chemical exchange reaction with an activation energy of 119 kJ mol^{-1}. This activation energy is in line with the reported value for anhydride formation.[30] In theory, this formation can be achieved both intramolecularly through neighboring group participation (NGP) or intermolecularly between two different phthalic bis(monoesters) (**Scheme 2**).

The relaxation behavior of the network was further studied by a temperature sweep experiment as shown in Figure 3C. The ramp shows that the material is cross-linked but gradually turns into a polymer melt where the storage modulus *G'* decreases after the rubber plateau starting at ≈140 °C. This type of relaxation of a covalently cross-linked network indicates a dissociative mechanism. The opening and closing of the anhydride by the reaction of free hydroxy group is a thermally driven equilibrium that exists in two states, either open as a diacid/bis(monoester) or closed as an anhydride. At low temperatures, the open state is favored, where an alcohol will open the anhydride ring to yield a monoester in an exothermic reaction as well as release ring strain of the five-membered anhydride ring, as observed by the initial network formation. At higher temperatures, the endothermic anhydride formation becomes favored, and the alcohol group is released again. The effect of the *o*-carboxylic acid as neighboring group in catalyzing the ring-closure of phthalic acid to phthalic anhydride was shown several years ago.[40,41] In our case, the *o*-carboxylic acid groups within the network can also act both as catalysts (Scheme 2) and as reagents. They can attack the carbonyl carbon of the ester units in the network, causing cleavage of the —C(O)—O— ester bond and generating anhydride and free hydroxyl groups. In contrast to the small organic molecules, this reaction in the network may proceed via intramolecular ring-closed anhydride formation, where the *o*-carboxylic acid reacts with a neighboring ester, or via intermolecular anhydride formation, where it reacts with ester bonds in another macromolecular chain. Bond reformation then occurs through the reaction of anhydrides with free hydroxyl groups. Vitrimers are contrary in this regard because they follow an associative mechanism where the rubbery plateau remains at a constant value due to the constant number of bonds at all temperatures. The rubbery plateau itself ranges from 80 to ≈140 °C at a storage modulus value of ≈3.3×10^5 Pa. The T_g derived from the loss modulus *G″* is in line with previously DSC determined one at ≈60 °C. The approximate cross-link density can also be derived from the rubbery plateau modulus under the assumption that no bond exchange takes place at the given temperature. The calculation results in a cross-link density of 105.4 mol m^{-3} or 0.1 mmol cm^{-3} considering the plateau at 100 °C (see p. S7, Supporting Information).[42] This value falls within the range of cross-linked elastomers ranging

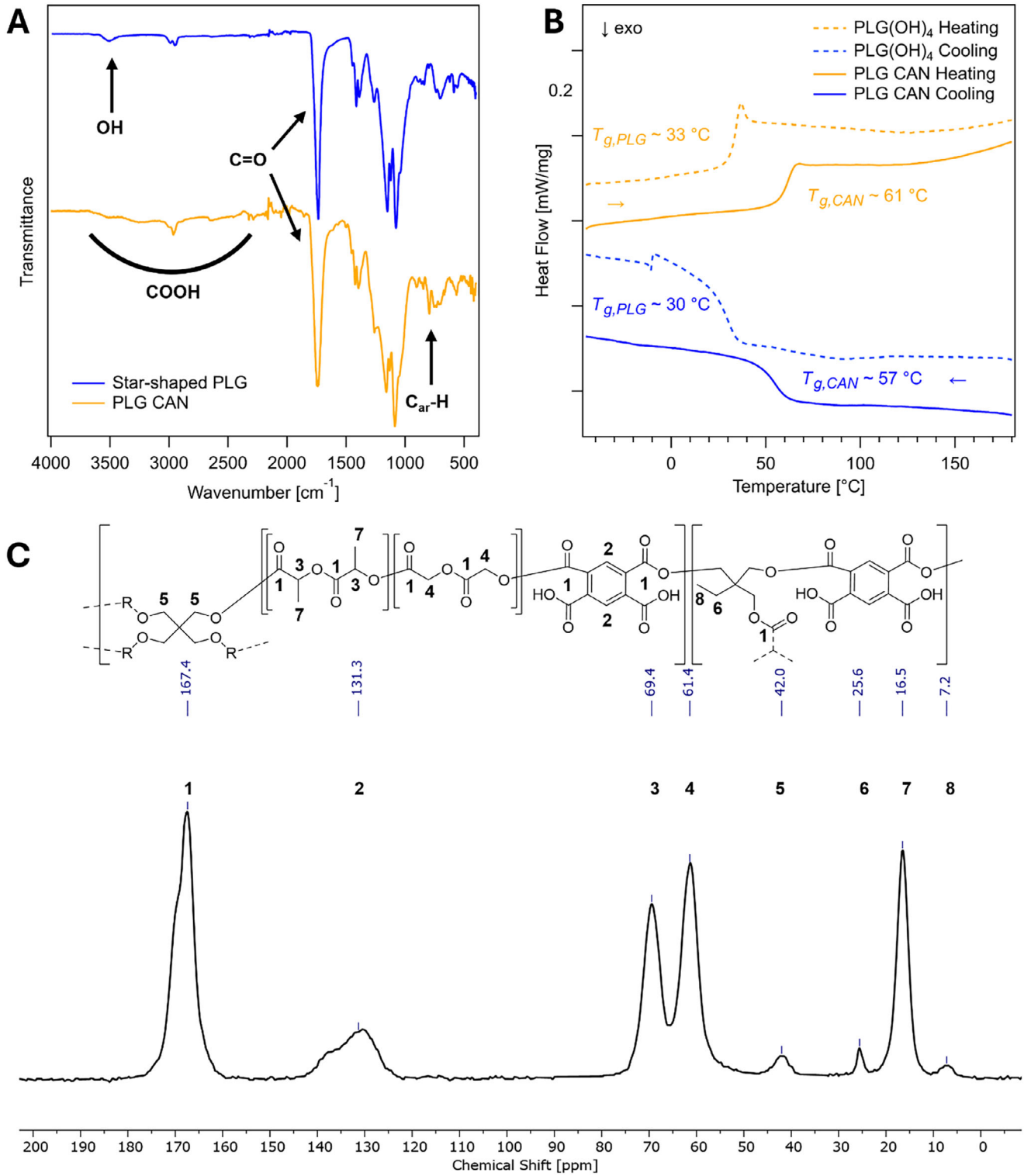

Figure 2. A) FTIR transmission spectrum of PLG macromonomer and PLG CAN including indication of the relevant functional groups. The spectra are normalized to the dominant carbonyl absorption at ≈1750 cm^{-1}. B) DSC second heating and cooling curves of PLG macromonomer and PLG CAN with 10 K min^{-1} heating rate and indication of glass transition temperatures. C) Solid-state ^{13}C-NMR of PLG CAN recorded at 100 MHz.

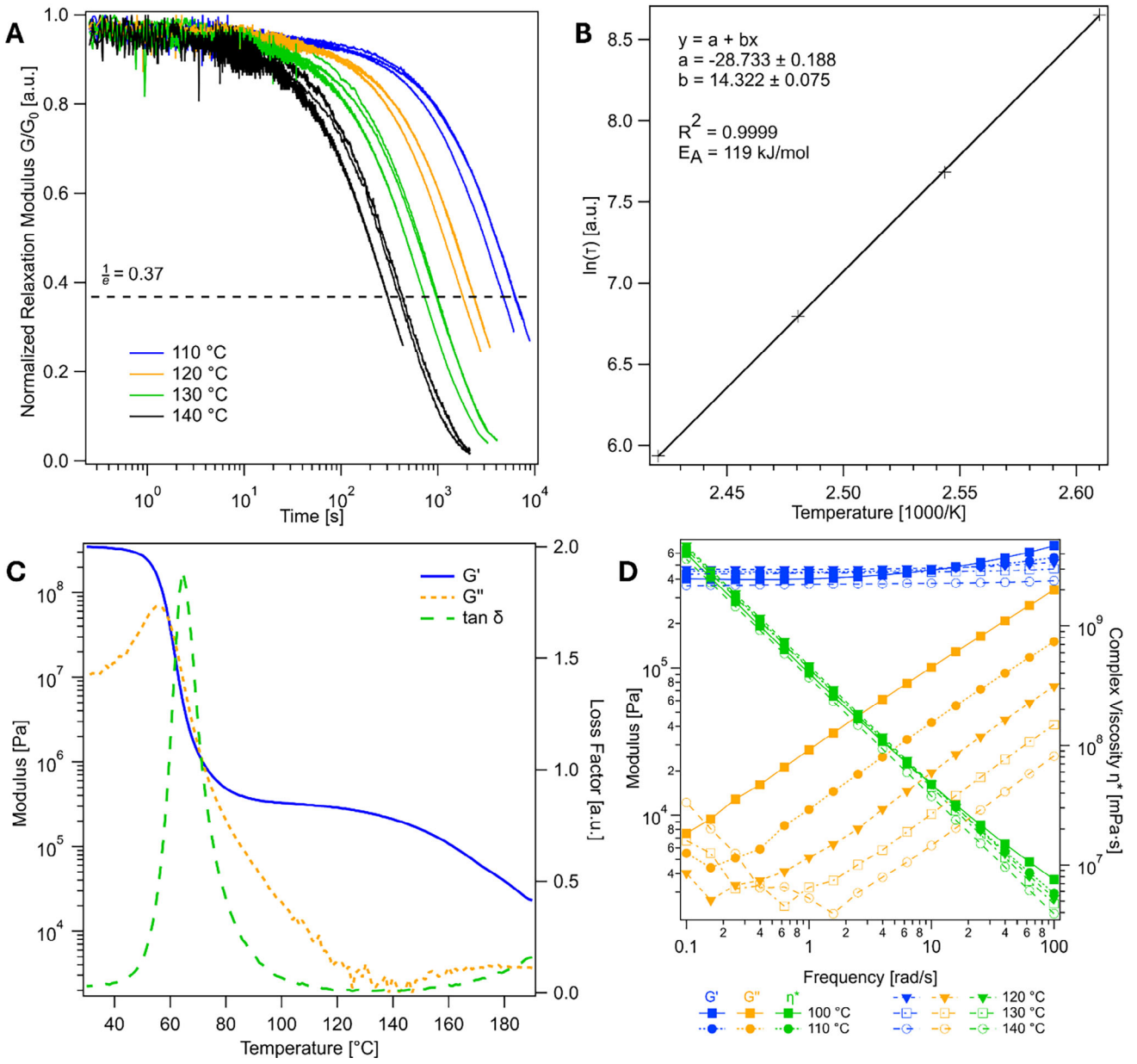

Figure 3. A) Normalized relaxation curves of PLG CAN at different temperatures under constant 0.5% shear, B) Arrhenius fit resulting from relaxation time values of 37% of the initial relaxation modulus, including fitting parameters and the activation energy, C) temperature ramp of PLG CAN from 190–35 °C at 2 K min^{-1}, and D) frequency sweeps at different temperatures.

from 50–200 mol m^{-3}, whereas high-performance thermosets show values of >500 mol m^{-3}.[43–45] Frequency sweeps, depicted in Figure 3D, were carried out to get further insights into the materials viscoelastic properties. At the rubbery plateau *G'* remains greater than *G″* throughout all frequencies, so no significant relaxation processes take place at varied frequency timescales, the material acts as an elastic solid. *G″* increases at higher frequencies, this indicates that energy is dissipated on a molecular level with resulting internal friction and may also include the mobility of defects, such as loose ends. The material acts overall as a solid and does not show relaxation behavior in the rubbery plateau at the given timescale. This proves the cross-linked nature of the reported network and its adaptable nature, enabled by dissociative bond exchanges through the dianhydride linker, at higher temperatures.

The PLG CAN was initially processed into 0.2 mm films using hot pressing (Figure S7, Supporting Information). The gel content, as derived by Equations (1) and (3), is calculated to be 94 ± 1%. The obtained dog-bone samples after punching from the hot-pressed films were analyzed in uniaxial tensile testing. The broken samples were cut into smaller pieces and reprocessed. The total processing time was halved for recycling to 20 min. The samples were again punched from the resulting film and analyzed again. The results depicted in Figure S6 (Supporting

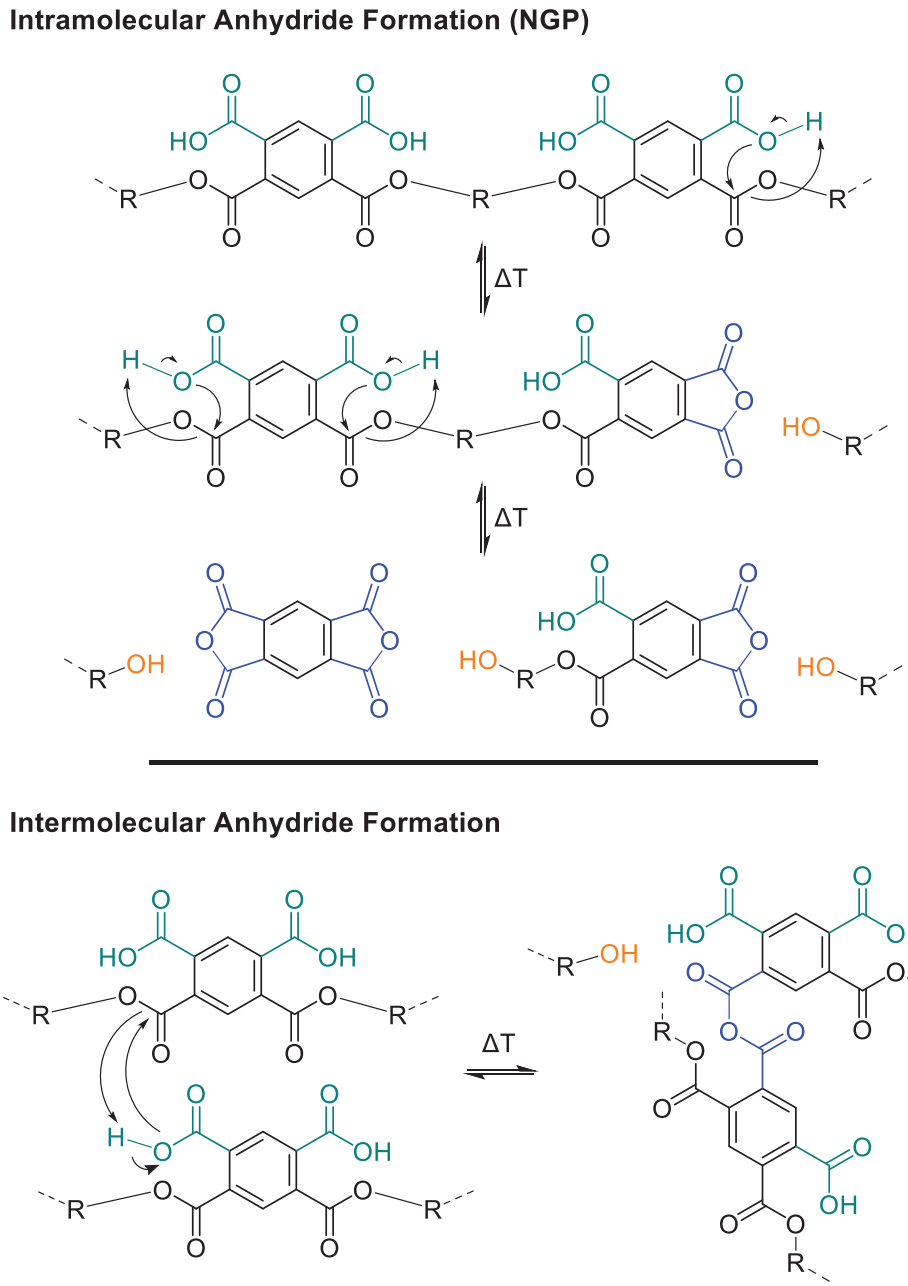

Scheme 2. Thermally activated mechanism of bond exchange reaction in PLG CANs. The dissociated network reforms at lower temperatures and reestablishes the bis(phthalic monoester) functional groups. In theory, both intra- and intermolecular anhydride formation is possible in polymer networks. Due to the neighboring group participation (NGP) intramolecular anhydride formation is more likely to occur. Anhydride formation in the network can also be incomplete leaving some esters intact during bond exchange reactions.

Information). All results are summarized in **Table 1**. The material can be thermally recycled under optimized processing conditions to retain its network integrity. The Youngs modulus $E_{mod,}$ remains unchanged at 1.6 GPa after recycling. This stiffness is comparable to well-known commercially available thermoplastic polyester, poly(L-lactide) (PLLA).

There could be several different applications of PLG CAN including the use as reusable adhesive. To study this possibility, PLG CAN film was placed between two metal sheets by heating

Table 1. Summary of mechanical properties of neat and recycled PLG CAN films compared to films prepared from commercial PLLA pellets.

Sample	E_{mod} [GPa]	ε_{max} [%]	F_{max} [MPa]
PLG CAN	1.6 ± 0.3	5.3 ± 3.0	33 ± 5.6
PLG CAN recycled	1.6 ± 0.1	1.3 ± 0.2	17 ± 3.0
PLLA[a)]	1.7 ± 0.1	12 ± 9.0	54 ± 1.5

[a)] Obtained from PLLA pellets processed to film (0.2 mm) at 200 °C.

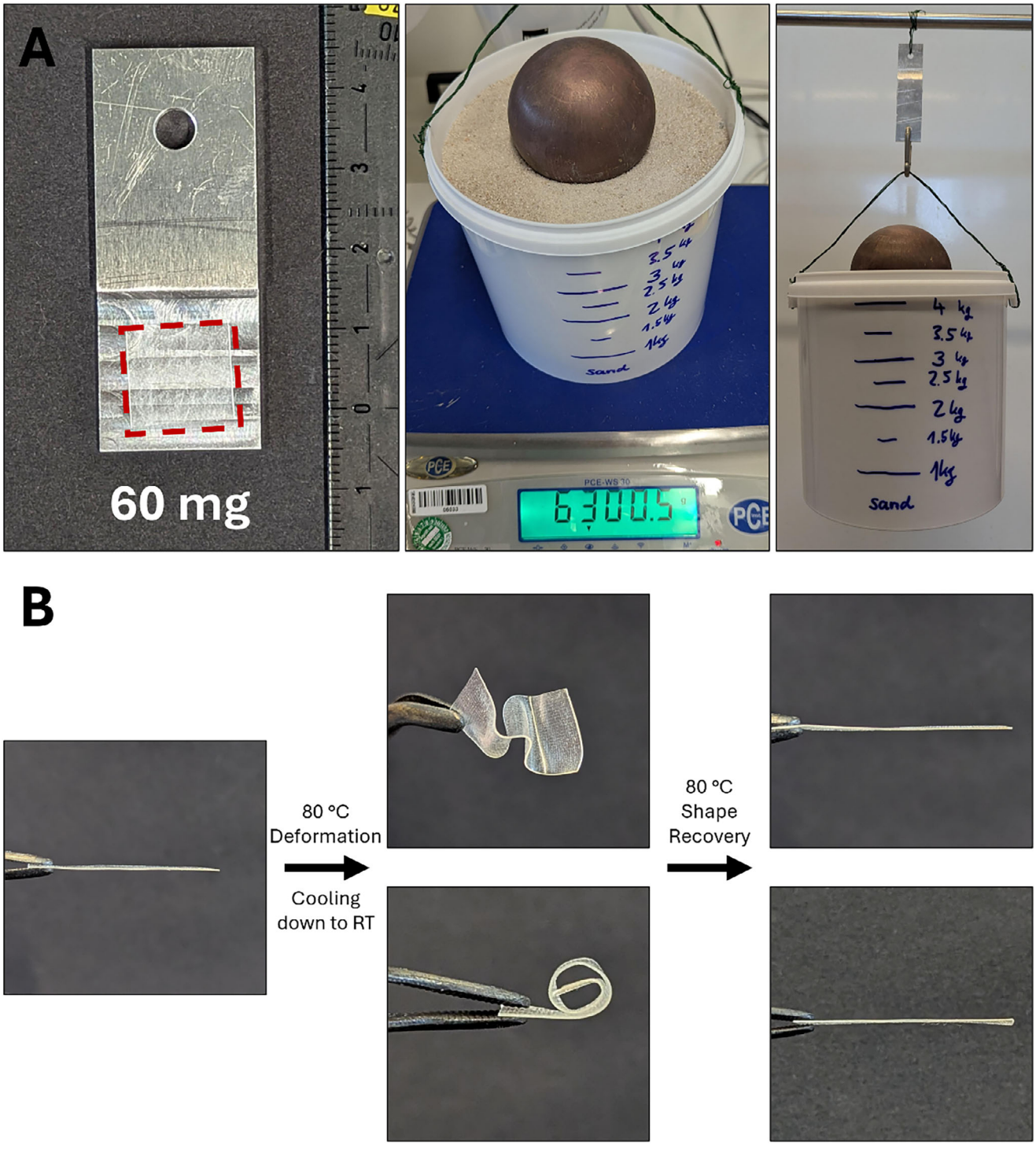

Figure 4. A) Weight test with a prepared metal sheet sample. A square piece of PLG CAN is pressed between two aluminum plates at 150 °C before axial stress is applied with varying weights. B) Demonstration of the one-way shape memory effect of the PLG CAN.

under pressure. The adhesion strength was tested by hanging varying weights off the plate assembly (**Figure** 4A). The film has a mass of 60 mg and can easily hold 6.3 kg for over 20 min on its first use without failure, corresponding to an adhesive strength of ≈618 kPa with an adhesive area of 1 cm^2 (p. S7, Supporting Information). This performance is comparable to pressure-sensitive adhesives (kPa range) and represents a promising strength-to-weight ratio for a (bio)degradable system demonstrating decent performance for temporary adhesive applications, particularly considering its recyclability and biodegradability advantages.[46]

During the second and third test cycle the same weight was held for over 20 min each time without failure. The film can be fully recovered without leaving any residue on the glued surface and can maintain its strength throughout multiple cycles. Another interesting property of PLG CAN is its one-way shape memory. The films become very flexible when heated above the T_g of ≈60 °C and can be easily reshaped. When cooled down the shape is kept and frozen. After reheating the initial film is fully recovered without changes (Figure 4B). This cycle can be repeated multiple times without any notable changes to the material such as cracks or other defects. The presented material has the potential to be used as a fully recoverable biodegradable adhesive film that also exhibits shape-memory. One-way shape-memory in PLG CANs provide dual functionality, bond exchange dynamics for reprocessability, shape memory for programmed deformation recovery. This combination can be useful for various purposes, such as packaging that shrinks at the end of its life, where the dynamic chemistry further allows chemical recyclability or reshaping instead of disposal. Other potential applications include reconfigurable 3D-printed parts and self-fitting components, among many others.

The degradability of the network as well as the macromonomer PLG was investigated under compost conditions using ISO 14855 (see p. S8, Supporting Information for compost composition). The incubation period was set to 60 days at 58 °C and the released CO_2 is continuously monitored and quantified. Each sample is measured in duplicates to ensure reproducibility. The theoretical biodegradation is calculated after determining the total organic carbon content of each sample (Equation 4). Sodium benzoate is measured as a fully degradable positive standard, validating the degradation experiment. The PLG CAN was used as film and cut into 1 × 1 cm rectangular pieces. They were evenly scattered in the sieved compost and buried. PLG macromonomer was also tested for its compostability in powder form. The degradation data is displayed in **Figure 5**.

After just 25 days the PLG macromonomer reaches up to 56% and the PLG CAN over 60% biodegradation, indicating that both materials do degrade fast under the given conditions. After 60 days sample PLG CAN 1 already shows ≈90% degradation. The network degrades faster and reaches 50% after just ≈10 days without an initial lag phase, PLG starts degrading after one day of lag. The enhanced biodegradation of the PLG CAN can be attributed to multiple synergistic factors. First, the PMDA cross-linking introduces carboxylic acid groups that act as both hydrophilic sites for water uptake and catalytic sites for ester bond hydrolysis. The result is a faster hydrolysis of the polyester backbone. Literature also suggests that the incorporation of acid groups has a positive impact on the degradability of polymers.[47–49] The rapid initial degradation suggests good compatibility with industrial composting conditions. Further testing in other media (soil, seawater, freshwater, etc.) would provide a more comprehensive degradation profile that is in progress.

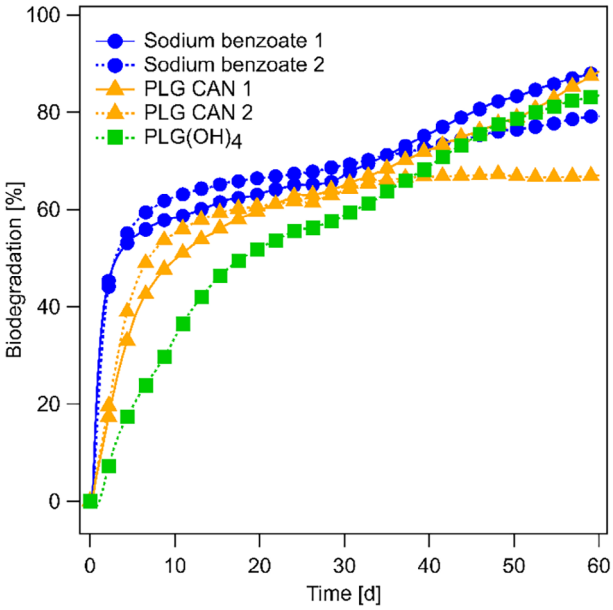

Figure 5. Biodegradation data of PLG CAN and PLG macromonomer in compost at 58 °C. Sodium benzoate is measured as a positive control. Biodegradation percentage calculated from CO_2 evolution relative to theoretical CO_2 production from total organic carbon content.

3. Conclusion

In this work, a catalyst-free covalent adaptable network based on star-shaped poly(lactide-*co*-glycolide) and pyromellitic dianhydride cross-linker was synthesized and characterized. The resulting PLG CAN exhibited a high gel content (up to 95%) and mechanical properties comparable to commercial P*L*LA, with a Young's modulus of ≈1.6 GPa. Stress relaxation analysis confirmed network adaptability, revealing an activation energy of 119 kJ mol^{-1}, consistent with the expected bond exchange reaction and literature. The material demonstrated rapid and extensive biodegradation under industrial composting conditions, with the network reaching over 60% degradation within 25 days, meeting the criteria for industrial composting (ISO 14855). Incorporation of carboxylic acid groups enhanced hydrolysis and accelerated biodegradation. Potential applications such as reusable adhesives and shape-memory materials were validated, showing robust adhesion (>6 kg load per 60 mg film) and repeatable one-way shape-memory response.

Overall, catalyst-free PLG CAN combines recyclability, robust mechanical performance, and proven biodegradability in compost. These properties position it as a promising candidate for sustainable polymer applications in a range of areas, including adhesives, advanced packaging, or biomedicine. Future work should investigate degradation behavior in various environmental conditions and optimize processing parameters to enhance recyclability. Additionally, exploration of other potential applications beyond adhesives and packaging materials would be valuable. Moreover, successful recycling without significant loss of properties over multiple cycles, the reduction of material brittleness, and processing under milder conditions should be achieved in future work.

4. Experimental Section

Materials: Pentaerythritol (PETL) (98%, Sigma–Aldrich), glycolide (97%, BLD Pharm), and pyromellitic dianhydride (PMDA) were purified by sublimation before use. *DL*-lactide (Corbion), benzoyl chloride (BzCl) (>99%, Thermo Fisher Scientific), pyridine (> = 99.5%, Thermo Fisher

Scientific), dimethyl amino pyridine (DMAP) (> = 99%, Fluka), and 2-ethyl-2-(hydroxymethyl)-1,3-propandiol (TMP) (for synthesis, Merck) were used as received. Tin(II) octoate ($Sn(Oct)_2$) (>92.5%, Sigma–Aldritch) was used as a 0.1 M stock solution in dry chloroform. Dry destabilized chloroform was prepared by first shaking it thoroughly with water to remove ethanol. This was followed by drying over calcium hydride and distillation. Tetrahydrofuran (THF) was destabilized and dried twice, first on calcium hydride then potassium, before distillation. Other used solvents were distilled before use. Deuterated chloroform (99.8%, Deutero GmbH) was dried and stored over 3 Å molecular sieves.

Synthesis of Star-Shaped Poly(Lactide-co-Glycolide): *DL*-lactide (7.93 g, 55 mmol, 12.5 eq), glycolide (6.38 g, 55 mmol, 12.5 eq), PETL (0.6 g, 4.4 mmol, 1 eq), and 176 µL $Sn(Oct)_2$ stock solution (0.1 M, 17.6 µmol, 0.004 eq) were mixed in a dried and silylated glass pressure tube equipped with a magnetic stir bar. The tube was flushed thoroughly with argon and sealed, before being wrapped into aluminum foil for thermal insulation. The tube was submerged in a preheated oil bath at 160 °C to ensure homogeneous heating of the entire reaction volume. After 3 h, an additional 2.14 g of glycolide (18.48 mmol, 4.2 eq) was added, and the reaction continued under the same conditions for another hour. When the reaction was finished, it was cooled to room temperature and the contents were dissolved in 75 mL dichloromethane (DCM). The first precipitation was carried out in pre-cooled methanol (−30 °C), resulting in the rapid agglomeration of polymer into a gum-like mass. The supernatant milky solution was decanted off and discarded. The polymer was washed twice with 20 mL fresh methanol and dissolved in 25 mL DCM. The second precipitation was done in cooled *n*-pentane (0 °C). Two different solvent types were used to precipitate the polymer in order to remove both polar and nonpolar impurities. During the first precipitation in methanol, polar contaminants were removed, whereas in the subsequent precipitation in nonpolar *n*-pentane, nonpolar impurities were eliminated. The solvent was removed and the polymer dried *in vacuo* at 70 °C for 16 h. The polymer was obtained as a colorless solid in ≈70% yield.

Synthesis of PLG Network: Star-shaped PLG (11.17 g, ≈3300 g mol^{-1}, 3.38 mmol, 1 eq), TMP (527 mg, 3.92 mmol, 1.16 eq), PMDA (2.76 g, 12.64 mmol, 3.74 eq), and ≈5 mg DMAP (catalytic amounts, ≈0.004 eq) were mixed in 65 mL dry THF in a dry and silylated Schlenk flask under argon. Everything was dissolved at 50 °C and afterward refluxed for 2 h at 80 °C (oil bath temperature). Excess solvent was removed by removing the reflux condenser, opening the flask, and evaporating the solvent off in a constant flow of argon and constant stirring. The flask was closed again, once the viscosity of the mixture reached a honey-like consistency. A gel was formed by letting the reaction carry on at 80 °C (oil bath temperature) for 48 h under argon. After the gel was formed it was cut into smaller pieces and extracted at 50 °C in 60 mL THF for 3 h. The polymer gel was filtered off and dried at 65 °C for 16 h *in vacuo*. The dried pieces were crushed in an electrical grinder after cooling them with liquid nitrogen. The crushed polymer network was dried at 80 °C for 16 h *in vacuo* followed by another drying step for 3 h at 120 °C *in vacuo*. The dried colorless polymer network was obtained in 93% yield.

OH-Group Quantification by "Einhorn"-Acylation: Star-shaped PLG (200 mg, ≈3300 g mol^{-1}, 0.06 mmol, 1 eq), pyridine (54 µL, 0.67 mmol, 0.982 g mL^{-1}, 11.1 eq), benzoyl chloride (63 µL, 0.54 mmol, 1.211 g mL^{-1}, 9 eq), and catalytic amounts of DMAP (0.004 eq) were dissolved and mixed in 5 mL dry chloroform. The reaction was stirred at 50 °C for 24 h. The reaction mixture was transferred into a centrifugal tube and precipitated by adding 40 mL of pre-cooled methanol (−30 °C), before centrifugation for 10 min at 10 °C and 8000 rpm. Any excess solvent was discarded and the polymer dried at 65 °C for 16 h *in vacuo*. The polymer was obtained in quantitative yield as a colorless solid.[50]

Polymer Film and Sample Preparation: Films and rheology samples were prepared by heat pressing on a Carver 2518 hot press at 150 °C upper and lower plate temperature, 3 t pressure, and 40 min pressing time. Films were prepared by placing the polymer material between two metal sheets and nonstick Kapton foil on each side. The thickness was controlled by using a brass frame with 0.2 mm thickness, this also prevented material from leaking into the press. Round rheology disc samples with 12 mm diameter and 1 mm thickness were prepared by using a custom mold. The pressure is removed after the given time and the sample including the metal plates is placed in a cooled press to completely cool down. Constant pressure of 20–30 kN was applied to prevent morphing. Dog-bone samples for tensile testing were punched from films using a Coesfeld hydraulic punching machine equipped with a DIN53504 S3A sample stencil. The films were heated using a heat gun to soften the material before punching the samples.

Thermal Reprocessing: Processed films were cut into small pieces and reprocessed on a Carver 2518 hot press at 150 °C for 20 min at 3 t pressure. Afterward the pressed films were put into a cooling press and cooled down at a pressure of 20–30 kN to prevent morphing. Dog-bone samples (DIN53504 S3A) were obtained using a Coesfeld hydraulic punching machine on the heated films.

Gel Content Determination: The soluble portion of the polymer was calculated using a straightforward solvent extraction technique at room temperature. A rectangular section of the processed polymer film, measuring ≈0.5 × 0.5 cm, was immersed in 10 mL of THF and subjected to gentle agitation over a duration of 24 h. In general, the solvent used for extraction should be able to dissolve all non-cross-linked components. The mass of the film in its initial (m_i), swollen (m_s), and dried states (m_d) were measured. The following equations were used to determine the soluble fraction (β), swelling ratio (ζ), and gel content (η):

$$\beta = \frac{m_i - m_d}{m_i} \tag{1}$$

$$\zeta = \frac{m_s - m_i}{m_i} \tag{2}$$

$$\eta = 100\% - \beta \tag{3}$$

Structural Analytical Methods: Structural features were measured on a PerkinElmer Spectrum Two attenuated total reflection Fourier transform infrared spectrometer (ATR FTIR). The measurements were conducted in the mid-infrared region, 450–4000 cm^{-1}, with a resolution of 4 cm^{-1}, and a total of four scans per sample to reduce the signal-to-noise ratio. All measurements were conducted at room temperature. Further analysis was carried out using solid-state nuclear magnetic resonance spectroscopy (NMR). The experiments were done on a Bruker 400 MHz MAS NMR with 3.2 mm sample probes. ^{1}H and ^{13}C experiments were conducted at a spinning frequency of 12.5 kHz at 400 and 100 MHz, respectively, cross-polarization was used for ^{13}C. The spectra were indirectly referenced with adamantane in relation to tetramethylsilane. Solution ^{1}H and ^{13}C-NMR were obtained on a Bruker Ultrashield 300 at room temperature at 300 and 75 MHz, respectively. Approximately 10 mg of the sample was dissolved in 0.8 mL of dry $CDCl_3$.

Thermogravimetric Analysis (TGA): TGA was carried out on a Netzsch TG 209 F1 Libra instrument under both air and nitrogen atmosphere. The samples were heated from 25 to 600 °C at a rate of 10 K min^{-1} in pierced lid 40 µL aluminum crucibles. A constant gas flow of 50 mL min^{-1} of 5.3 nitrogen or synthetic air was maintained. Approximately 5–10 mg were used per measurement.

Differential Scanning Calorimetry (DSC): Thermal characteristics were performed on a Netzsch DSC 204 F1 Phoenix instrument. 5–10 mg of each sample were put into 40 µL aluminum crucibles and closed with pierced lids. The measurements were performed from −50 to 200 °C with a heating rate of 10 K min^{-1} and a constant gas flow of 20 mL min^{-1} nitrogen 5.3. The glass transition temperature was taken from the second heating curve.

Gel Permeation Chromatography (GPC): The experiments were performed on a SDV linear XL gel column with a separation range of 100 to $3{\cdot}10^6$ Da. A refractive index detector (Agilent Technologies 1200 series) was used. The used eluent was chloroform (HPLC-standard grade) with a flow rate of 0.5 mL min^{-1} at room temperature. Toluene is used as an internal standard. The calibration was performed with narrowly distributed poly(styrene) homopolymer (PSS calibration kit). The injection volume was 20 µL with a polymer concentration of 1 mg mL^{-1}. Prior to the measurement each sample was dissolved in chloroform and filtered through a PTFE filter with 0.2 mm pore size.

Rheology: Stress-relaxation analysis (SRA) experiments were carried out on an Anton Paar MCR302 rheometer equipped with a P-TD 200 Peltier plate and a H-PTD 200 Peltier hood for temperatures below 200 °C. A plate-plate setup for 12 mm circular samples with a shaft for disposable measurements (D-CP/PP 7) and samples with 1 mm thickness were used. The samples were directly obtained from thermal processing. Prior to each relaxation experiment a strain sweep at the corresponding temperature was performed within 0.1 and 2 % strain to ensure the range of the linear viscoelastic regime. The relaxation experiments were performed under constant strain. Relaxation experiments were conducted at 110, 120, 130, and 140 °C. Each sample was allowed to equilibrate for at least 10 min at the given temperature and in between measurements. Stress decay was monitored until 37% of the initial relaxation plateau was reached. Full relaxation was recorded at 130 and 140 °C. Temperature ramps were performed on the same setup. The ramp was measured from 190 to 30 °C at a constant circular frequency of 1 Hz, with a logarithmic strain ramp from 0.5 % at high and 0.03 % at low temperatures, and a logarithmic applied force ramp of 0.05–2 N to ensure good contact of the samples and prevent slipping.

Uniaxial Tensile Testing: Uniaxial tensile testing was performed on both neat and recycled samples on a Zwick Roell Z0.5 tensile tester (BT1 FR 0.5TN-D14) with a 500 N KAF-TC force sensor. A standard measurement speed of 10 mm min^{-1} was used at varying preloads at a grip-to-grip separation of 20 mm at room temperature. The samples were equilibrated under measuring room conditions for at least 24 h. Before each measurement, the thickness of each sample was obtained by calculating the mean value from three points along the gauge area. Length and width of the samples were fixed at 16 and 4 mm, respectively, according to the sample geometry DIN53504 S3A. The elastic modulus was determined automatically from the slope of the linear region of the stress-strain curves. At least three measurements per sample were taken.

Degradation in Compost: The aerobic composting tests were executed according to ISO 14855 using a MicroOxymax Respirometer from Columbus Instruments. 12-week-old compost was picked up from the compost plant "*Am Buchstein*" in Bayreuth and sieved to < 1 cm. The pH-value, water and ash-content, as well as the total carbon and nitrogen content were analyzed post sieving. For the biodegradation test a ratio of 50:1 dry compost to sample was used (100 g dry compost to 2 g sample). To monitor the volume change in gas, blank compost samples were measured, and sodium benzoate was used as a positive standard. The samples were measured in duplicates or triplicates and incubated at 58 °C for 60 days. The accumulated CO_2 was determined via an IR-based sensor. The biodegradation (BD) was calculated via the following equation:

$$BD\,[\%] = \frac{CO_{2,sample} - CO_{2,blank}}{CO_{2,theo.}} \times 100\% \quad (4)$$

where $CO_{2,sample}$ and $CO_{2,blank}$ is the detected amount of CO_2 of the sample and the blank, respectively. $CO_{2,theo.}$ describes the theoretical amount of CO_2 accumulated at 100 % biodegradation of a respective sample. $CO_{2,theo.}$ can be calculated from the sample mass m_{sample}, the total carbon content of the sample *TOC* and the molar mass of CO_2 (M_{CO2}) and carbon (M_C):

$$CO_{2,theo.} = m_{sample} \times TOC \times \frac{M_{CO_2}}{M_C} \quad (5)$$

Adhesion Test: Rectangular film specimens (1 × 1 cm) were placed between two custom-made aluminum plates (2 mm thickness), each featuring a 1 mm smooth, milled adhesion surface. The assembled plate–film–plate system was placed onto a preheated hot plate set to 150 °C, and a 5 kg load was applied to the upper plate to ensure uniform pressure. After heating for 10 min, the assembly was removed from the hot plate and allowed to cool to room temperature. Adhesion strength was evaluated by incrementally suspending previously weighted masses from the free-hanging plate assembly. Each mass was applied for a minimum of 10 min before increasing to the next increment, usually 500 g. To remove the adhered film for another testing cycle, the sample was reheated on the hot plate, and the film was easily recovered. The heating time was increased to 20 min for the second and third adhesion test cycle.

Supporting Information

Supporting Information is available from the Wiley Online Library or from the author.

Acknowledgements

The authors would like to thank the Bavarian Polymer Institute at the University of Bayreuth, Germany, for allowing the use of the equipment in "Small Scale Polymer Processing" and "Synthesis and Molecular Characterization" Keylabs. The authors would also like to thank Beate Bojer of the chair of Inorganic Chemistry III of the University of Bayreuth, Germany, for providing solid-state NMR measurements. Deutsche Forschungsgemeinschaft (DFG, German Research Foundation)—project number 391977956, C02—SFB 1357 is also thanked for supporting the work.

Open access funding enabled and organized by Projekt DEAL.

Conflict of Interest

The authors declare no conflict of interest.

Data Availability Statement

The data that support the findings of this study are available in the supplementary material of this article.

Keywords

biodegradation, catalyst-free, covalent adaptable networks, cross-linked polymer, sustainability

Received: October 13, 2025
Revised: October 29, 2025
Published online:

[1] PlasticsEurope, Plastics - the fast Facts 2024, can be found under, https://plasticseurope.org/knowledge-hub/plastics-the-fast-facts-2024/2025.
[2] S. Utekar, S. V K, N. More, A. Rao, *Composites, Part B* **2021**, *207*, 108596.
[3] S. J. Pickering, *Composites, Part A* **2006**, *37*, 1206.
[4] E. Morici, N. T. Dintcheva, *Polymers* **2022**, *14*, 4153.
[5] C. J. Kloxin, T. F. Scott, B. J. Adzima, C. N. Bowman, *Macromolecules* **2010**, *43*, 2643.
[6] C. J. Kloxin, C. N. Bowman, *Chem. Soc. Rev.* **2013**, *42*, 7161.
[7] M. Capelot, D. Montarnal, F. Tournilhac, L. Leibler, *J. Am. Chem. Soc.* **2012**, *134*, 7664.
[8] K. Yu, P. Taynton, W. Zhang, M. L. Dunn, H. J. Qi, *RSC Adv.* **2014**, *4*, 10108.
[9] J. P. Brutman, P. A. Delgado, M. A. Hillmyer, *ACS Macro Lett.* **2014**, *3*, 607.
[10] X. Niu, F. Wang, X. Li, R. Zhang, Q. Wu, P. Sun, *Ind. Eng. Chem. Res.* **2019**, *58*, 5698.
[11] E. M. Eger, S. Agarwal, *ACS Appl. Polym. Mater.* **2023**, *5*, 5141.

[12] C. Bakkali-Hassani, D. Berne, V. Ladmiral, S. Caillol, *Macromolecules* **2022**, *55*, 7974.
[13] X. Chen, L. Li, K. Jin, J. M. Torkelson, *Polym. Chem.* **2017**, *8*, 6349.
[14] D. J. Fortman, J. P. Brutman, C. J. Cramer, M. A. Hillmyer, W. R. Dichtel, *J. Am. Chem. Soc.* **2015**, *137*, 14019.
[15] A. Chao, I. Negulescu, D. Zhang, *Macromolecules* **2016**, *49*, 6277.
[16] H. Memon, Y. Wei, L. Zhang, Q. Jiang, W. Liu, *Compos. Sci. Technol.* **2020**, *199*, 108314.
[17] W. Denissen, G. Rivero, R. Nicolaÿ, L. Leibler, J. M. Winne, F. E. Du Prez, *Adv. Funct. Mater.* **2015**, *25*, 2451.
[18] W. Denissen, M. Droesbeke, R. Nicolaÿ, L. Leibler, J. M. Winne, F. E. Du Prez, *Nat. Commun.* **2017**, *8*, 14857.
[19] C. Taplan, M. Guerre, J. M. Winne, F. E. Du Prez, *Mater. Horiz.* **2020**, *7*, 104.
[20] A. Ruiz de Luzuriaga, G. Solera, I. Azcarate-Ascasua, V. Boucher, H.-J. Grande, A. Rekondo, *Polymer* **2022**, *239*, 124457.
[21] N. Tratnik, N. R. Tanguy, N. Yan, *Chem. Eng. J.* **2023**, *451*, 138610.
[22] T. Debsharma, V. Amfilochiou, A. A. Wróblewska, I. de Baere, W. van Paepegem, F. E. Du Prez, *J. Am. Chem. Soc.* **2022**, *144*, 12280.
[23] C. Tretbar, J. Castro, K. Yokoyama, Z. Guan, *Adv. Mater.* **2023**, *35*, 2303280.
[24] J. L. Self, N. D. Dolinski, M. S. Zayas, J. Read de Alaniz, C. M. Bates, *ACS Macro Lett.* **2018**, *7*, 817.
[25] M. Concilio, G. S. Sulley, F. Vidal, S. Brown, C. K. Williams, *J. Am. Chem. Soc.* **2025**, *147*, 6492.
[26] S. Bhusal, C. Oh, Y. Kang, V. Varshney, Y. Ren, D. Nepal, A. Roy, G. Kedziora, *The J. Phys. Chem. B* **2021**, *125*, 2411.
[27] M. Hayashi, *ACS Appl. Polym. Mater.* **2020**, *2*, 5365.
[28] Y. Zhu, W. Li, Z. He, K. Zhang, X. Nie, R. Fu, J. Chen, *Polymers* **2024**, *16*, 307.
[29] A. Adjaoud, B. Marcolini, R. Dieden, L. Puchot, P. Verge, *J. Am. Chem. Soc.* **2024**, *146*, 13367.
[30] M. Delahaye, J. M. Winne, F. E. Du Prez, *J. Am. Chem. Soc.* **2019**, *141*, 15277.
[31] M. Capelot, M. M. Unterlass, F. Tournilhac, L. Leibler, *ACS Macro Lett.* **2012**, *1*, 789.
[32] E. Pamula, E. Menaszek, *Mater. Med.* **2008**, *19*, 2063.
[33] Y. Wang, M. A. Murcia Valderrama, R.-J. van Putten, C. J. E. Davey, A. Tietema, J. R. Parsons, B. Wang, G.-J. M. Gruter, *Polymers* **2021**, *14*, 15.
[34] A. R. Bagheri, C. Laforsch, A. Greiner, S. Agarwal, *Global challenges* **2017**, *1*, 1700048.
[35] G. Wypych, *Handbook of polymers*, CP ChemTec Publishing, Toronto, **2016**.
[36] S. Kaihara, S. Matsumura, A. G. Mikos, J. P. Fisher, *Nat. Protoc.* **2007**, *2*, 2767.
[37] P. in Pyo Park, S. Jonnalagadda, *J. Appl. Polymer Sci* **2006**, *100*, 1983.
[38] P. G. de Gennes, *J. Chem. Phys.* **1971**, *55*, 572.
[39] M. L. Williams, R. F. Landel, J. D. Ferry, *J. Am. Chem. Soc.* **1955**, *77*, 3701.
[40] M. L. Bender, F. Chloupek, M. C. Neveu, *J. Am. Chem. Soc.* **1958**, *80*, 5384.
[41] J. W. Thanassi, T. C. Bruice, *J. Am. Chem. Soc.* **1966**, *88*, 747.
[42] L. W. Hill, *Prog. Org. Coat.* **1997**, *31*, 235.
[43] J. Boden, C. R. Bowen, A. Buchard, M. G. Davidson, C. Norris, *ACS Omega* **2022**, *7*, 15098.
[44] J.-S. Chen, C. K. Ober, M. D. Poliks, Y. Zhang, U. Wiesner, C. Cohen, *Polymer* **2004**, *45*, 1939.
[45] N. Yazıcı, E. Opar, M. Kodal, B. Tanören, M. Sezen, G. Özkoç, *Polym. Polymer Comp.* **2022**, *30*, 09673911221074193.
[46] M. K. Danielson, B. G. Sumpter, Z. Demchuk, C. Gainaru, C. Pan, T. Saito, M. A. Rahman, *Sci. Adv.* **2025**, *11*, adw1288.
[47] R. S. Boethling, E. Sommer, D. DiFiore, *Chem. Rev.* **2007**, *107*, 2207.
[48] J. Li, R. M. Stayshich, T. Y. Meyer, *J. Am. Chem. Soc.* **2011**, *133*, 6910.
[49] C. Lin, H. Zhang, *Environ. Sci. Technol.* **2025**, *59*, 1253.
[50] A. Einhorn, F. Hollandt, *Ann. Chem* **1898**, *301*, 95.